

Reversible random sequential adsorption of mixtures on a triangular lattice

I. Lončarević and Lj. Budinski-Petković

Faculty of Engineering, Trg D. Obradovića 6, Novi Sad 21000, Serbia

S. B. Vrhovac*

Institute of Physics, P.O. Box 68, Zemun 11080, Belgrade, Serbia

(Received 22 March 2007; published 7 September 2007)

Reversible random sequential adsorption of binary mixtures of extended objects on a two-dimensional triangular lattice is studied numerically by means of Monte Carlo simulations. The depositing objects are formed by self-avoiding lattice steps. We concentrate here on the influence of the symmetry properties of the shapes on the kinetics of the adsorption-desorption processes in two-component mixtures. We provide a detailed discussion of the significance of collective events for governing the time coverage behavior of component shapes with different rotational symmetries. We also investigate the role that the mixture composition plays in the deposition process. For the mixtures of equal sized objects, we propose a simple formula for predicting the value of the steady-state coverage fraction of a mixture from the values of the steady-state coverage fractions of pure component shapes.

DOI: [10.1103/PhysRevE.76.031104](https://doi.org/10.1103/PhysRevE.76.031104)

PACS number(s): 02.50.-r, 68.43.Mn, 05.10.Ln, 05.70.Ln

I. INTRODUCTION

Random sequential adsorption (RSA) is a typical model for irreversible deposition of macromolecules and microscopic particles such as polymers, colloids, bacteria, protein or latex particles on solid surfaces. In this process objects are deposited randomly and sequentially onto a substrate. The depositing particles are not allowed to overlap with the previously deposited ones and the adsorbed particles do not detach from the surface. RSA models are applied to processes for which the relaxation over typical observation times is negligible. See Evans [1] for a comprehensive survey. Recent surveys include Privman [2], Senger *et al.* [3], and Talbot *et al.* [4].

On the other hand, there is a number of physical processes that involve both adsorption and desorption of particles. Adsorption-desorption processes are important in the binding of ions to a Langmuir monolayer [5], the interaction of proteins with DNA [6], and in many catalytic reactions. Recently, there has been a renewed interest in the reversible RSA because of its successful application to compaction of granular materials. An adsorption-desorption model can reproduce qualitatively the slow density relaxation [7–9], memory effects [10,11] and other features of weakly vibrated granular materials.

Numerical results [12] for the single-layer irreversible deposition of objects of various shapes on a triangular lattice suggest that the approach to the jamming limit follows the exponential law with the rate dependent mostly on the order of symmetry axis of the shape. Recently, we have carried out the extensive simulations of reversible RSA using objects of different sizes and rotational symmetries on a triangular lattice [8]. We have found that the growth of the coverage $\theta(t)$ above the jamming limit θ_{jam} to its steady-state value θ_{∞} is described by a pattern $\theta(t) = \theta_{\infty} - \Delta \theta E_{\beta}[-(t/\tau)^{\beta}]$, where E_{β}

denotes the Mittag-Leffler function of order $\beta \in (0, 1)$ [13]. Parameters τ , β , θ_{∞} , and $\Delta \theta \approx \theta_{\infty} - \theta_{\text{jam}}$ are the fitting parameters. Parameter τ determines the characteristic time of the coverage evolution and β measures the rate of deposition process on this time scale. The parameter τ is found to decay with the desorption probability P_- according to a power law $\tau = AP_-^{-\gamma}$. Exponent γ is the same for all the shapes, but parameter A depends only on the order of symmetry axis of the shape. This established the crucial role of the geometrical character and symmetry properties of the extended objects in the reversible RSA dynamics.

Particles in nature, such as colloidal and bioparticles, are not monodisperse. Because their sizes and shapes vary considerably, polydispersity is almost an inevitable property in many experimental situations. The binary mixture is the simplest and the first step toward the understanding of polydisperse systems. In this paper we present the results of Monte Carlo simulations for the reversible RSA of a two-component mixture of extended objects on a triangular lattice. Simulations are performed for objects of various shapes. The depositing objects are modeled by self-avoiding walks on the two-dimensional triangular lattice. A self-avoiding shape of length ℓ is a sequence of *distinct* vertices $(\omega_0, \dots, \omega_{\ell})$ such that each vertex is a nearest neighbor of its predecessor, i.e., a walk of length ℓ covers $\ell + 1$ lattice sites. Examples of such walks for $\ell = 1, \dots, 6$ are shown in Table I. On a triangular lattice objects with a symmetry axis of first, second, third, and sixth order can be formed. Rotational symmetry of order n_s , also called n -fold rotational symmetry, with respect to a particular axis perpendicular to the triangular lattice, means that rotation by an angle of $2\pi/n_s$ does not change the object. We concentrate here on the influence of the order of symmetry axis of the shape on the kinetics of the adsorption-desorption processes in two-component mixtures. Special attention is paid to the mixtures of lattice objects of different rotational symmetries but of the same number of segments. We find that the mixtures exhibit a behavior that is qualitatively different from the monodisperse adsorption.

*vrhovac@phy.bg.ac.yu; <http://www.phy.bg.ac.yu/~vrhovac/>

TABLE I. Coverage fraction $\theta_{jam}^{(x)}$ for various shapes (x) of length $\ell^{(x)}$ on a triangular lattice. The colors (online only) are associated with the different order $n_s^{(x)}$ of symmetry axis.

(x)	shape	$n_s^{(x)}$	$\ell^{(x)}$	$\theta_{jam}^{(x)}$
(A)		2	1	0.9140
(B)		2		0.8362
(C)		1	2	0.8345
(D)		3		0.7970
(E)		2	3	0.7886
(F)		3		0.7212
(G)		6	5	0.5740
(H)		1		0.6761
(I)		2		0.7214
(J)		6	6	0.6695
(K)		1		0.6443

The paper is organized as follows. Section II describes the details of the simulations. We give the simulation results and discussions in Sec. III and IV. Finally, Sec. V contains some additional comments and final remarks.

II. DEFINITION OF THE MODEL AND THE SIMULATION METHOD

The process that we have investigated in this paper consists of the random deposition and desorption of extended objects from Table I on a triangular lattice of size $L=120$. Periodic boundary conditions are used along all directions. Consider a two-component mixture of objects (A) and (B) with the symmetry axis of $n_s^{(A)}$ and $n_s^{(B)}$ order, respectively. The reversible RSA process for a binary mixture is as follows. From a large reservoir of shapes, that contains the

shapes (A) and (B) with the fractional concentrations $r^{(A)}$ and $r^{(B)}=1-r^{(A)}$, we choose one shape at random. The concentrations $r^{(A)}$ and $r^{(B)}$ are unaffected by adsorption or desorption events. We randomly select a lattice site and try to deposit the chosen shape of length ℓ with probability P_+ . If the selected site is occupied by a deposited object the adsorption attempt is rejected. If the selected site is unoccupied, we fix the beginning of the walk that makes the chosen shape at this site. Then we randomly pick one of the six possible orientations with equal probability, start the corresponding ℓ -step walk in that direction and search whether all successive ℓ sites are unoccupied. If so, we occupy these $\ell+1$ sites and deposit the object; otherwise, the deposition attempt is rejected. Each adsorption attempt is followed by a desorption one with probability P_- . Desorption process starts by choosing a lattice site at random. If this selected site is unoccupied, the desorption step fails and the process continues by choosing a new site for adsorption attempt. On the other hand, if the selected site is occupied by an adsorbed object, the object is removed from the lattice. The kinetics of the adsorption-desorption model depends only on the ratio $K=P_+/P_-$. In order to save the computer time it is convenient to take the adsorption probability to be $P_+=1$, i.e., to try an adsorption at each Monte Carlo step.

The time t is counted by the number of adsorption attempts and scaled by the total number of lattice sites L^2 . The quantity of interest is the fraction of total lattice sites, $\theta^{(A)+(B)}(t)$, covered by the deposited objects (A) and (B) at time t . Let $\theta^{(A)}(t)$ and $\theta^{(B)}(t)$ denote the coverage fraction of each species adsorbed at time t . The output data are averaged over 100 independent runs for each choice of mixture and each desorption probability P_- . A more detailed description of the numerical procedure used in our simulation has been given elsewhere [8].

Without desorption, the deposition process ceases when all unoccupied spaces on the lattice are smaller than the size of an adsorbed object. The system is then jammed in a non-equilibrium disordered state. When the deposited particles are subjected to desorption, the system formed by the adsorbed objects on the lattice can reach an equilibrium state. In the reversible case, the process reaches a steady state in which the rate of adsorption is exactly balanced by the rate of desorption. In this paper, θ_∞ will designate the steady-state value of the fractional coverage, and θ_{jam} will refer to θ_∞ in the case $P_-=0$, i.e., the jamming limit. During the simulation of irreversible deposition we record the number of inaccessible sites in the lattice. A site is inaccessible if it is occupied or it cannot be the beginning of neither of the shapes making the mixture. The jamming limit is reached when the number of inaccessible sites is equal to the total number of lattice sites.

For the lattice models, the asymptotic approach of the coverage fraction $\theta(t)$ to its jamming limit θ_{jam} is known to be given by the exponential time dependence [14,15],

$$\theta(t) \sim \theta_{jam} - \Delta\theta \exp(-t/\sigma), \quad (2.1)$$

where $\Delta\theta$ and σ are parameters that depend on the shape and orientational freedom of depositing objects [12,16]. The shapes with the symmetry axis of a higher order have lower

TABLE II. Coverage fraction $\theta_{\text{jam}}^{(x)+(y)}$ for various binary mixtures $(x)+(y)$ of shapes (A)–(K) from Table I. The colors (online only) are associated with the different order $n_s^{(x)}$ of symmetry axis. Jamming coverages shown are for $r^{(x)}=r^{(y)}=1/2$.

$(x)+(y)$	shapes	$n_s^{(x)}+n_s^{(y)}$	$\ell^{(x)}+\ell^{(y)}$	$\theta_{\text{jam}}^{(x)+(y)}$
(B)+(C)		2+1	2+2	0.8526
(C)+(D)		1+3	2+2	0.8624
(B)+(D)		2+3	2+2	0.8591
(F)+(G)		3+6	5+5	0.6833
(I)+(J)		2+6	6+6	0.7125
(J)+(K)		6+1	6+6	0.7087
(A)+(B)		2+2	1+2	0.9202
(A)+(E)		2+2	1+3	0.9191
(J)+(H)		6+1	6+5	0.7085

values of σ , i.e., they approach their jamming limit more rapidly. The parameter $\Delta\theta$ decreases with the object size for the same type of shape.

Measured values for the jamming coverage θ_{jam} resulting from the irreversible RSA of pure lattice shapes onto a triangular lattice are given in Table I. The results show a strong dependence of the jamming limit θ_{jam} on the shape of the adsorbed species. We note that the results in Table I for θ_{jam} differ from our previous estimates, e.g., [12].

In the present paper results are reported for the above-described conventional model of RSA, whereas in Ref. [12] we have used the end-on model of RSA. In the end-on model, the depositing shape always checks all possible directions from the selected site. If the object cannot be placed in any of the six orientations, this site is denoted as inaccessible. Therefore, the local domain structures for an end-on model are more dense than those of the conventional model. Consequently, the jamming limit for the end-on model is slightly larger than that for the conventional model.

The set of binary mixtures used in our simulations is shown in Table II. Each mixture $(x)+(y)$ is composed of two lattice objects (A)–(K) from Table I. The corresponding jamming coverages $\theta_{\text{jam}}^{(x)+(y)}$ for $r^{(x)}=r^{(y)}=1/2$ are also given in the last column of Table II.

III. DENSIFICATION KINETICS

Using the RSA algorithm defined in the preceding section extensive calculations were performed in order to determine the time evolution of the coverage fraction and the structure of the adsorbed layer. We investigate the role that the mixture composition and the symmetry properties of the shapes play in the deposition process. We will mainly concentrate on the case of binary mixtures, composed of the shapes of equal number of segments.

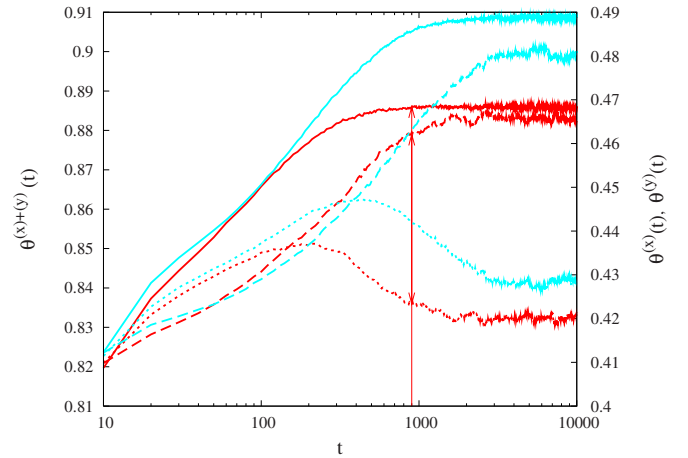


FIG. 1. (Color online) Shown here is the time dependence of the coverage fraction for mixture (B)+(C) (see Table II) and its components for $r^{(B)}=r^{(C)}=1/2$ and for two different values of desorption probability $P_-=0.002, 0.001$. Black (red) and gray (light blue) lines represent the results obtained for $P_-=0.002$ and 0.001 , respectively. The solid lines represent the temporal behavior of coverage fraction $\theta^{(B)+(C)}(t)$ (left-hand axis). The dashed and dotted lines are plotted against the right-hand axis and give the coverage fraction versus time t of component shapes (B), $\theta^{(B)}(t)$ (dashed line), and (C), $\theta^{(C)}(t)$ (dotted line). Thin vertical arrow indicates the beginning of the equilibrium plateau in the time evolution of the coverage fraction $\theta^{(B)+(C)}(t)$ for $P_-=0.002$.

The time behavior of the coverage fraction $\theta^{(x)+(y)}(t)$ for the first three mixtures $(x)+(y)=(B)+(C), (C)+(D), (B)+(D)$ in Table II are presented in Figs. 1–3, where two relatively low values of $P_-=0.002$ and 0.001 have been used. These mixtures are composed of the shapes of length $\ell=2$. The time evolution of $\theta^{(x)+(y)}(t)$ for low values of P_- shows a similar behavior for both the single-component systems [5,8,17,18] and for the mixtures. Indeed, the relaxation of the system toward its equilibrium coverage fraction $\theta_{\infty}^{(x)+(y)}$ is a two-stage process: at very early times of the process, when the coverage fraction is small, the adsorption process is dominant and the coverage grows rapidly in time; for large enough coverages ($\theta^{(x)+(y)}(t) > \theta_{\text{jam}}^{(x)+(y)}$) the growth of the coverage fraction $\theta^{(x)+(y)}(t)$ requires the rearrangement of the increasing number of particles in order to open a hole large enough for the insertion of an additional particle, and the role of desorption is crucial. This strongly suggests that the collective events are responsible for the evolution of $\theta^{(x)+(y)}(t)$ for $\theta^{(x)+(y)}(t) > \theta_{\text{jam}}^{(x)+(y)}$. Because these events involve the multiple particle transitions, they occur on a longer time scale than the simple adsorption-desorption events.

In contrast to the monodisperse case the analysis of collective processes is significantly more complex for the mixtures, because of the large variety of spatial arrangements corresponding to transitions that involve two and more two-dimensional shapes. However, we did carry out a detailed analysis of the contribution to the densification kinetics coming from each mixture component. Figure 1 shows the time dependence of the coverages $\theta^{(B)}(t)$ and $\theta^{(C)}(t)$ resulting from the reversible RSA of binary mixture of (B) and (C)

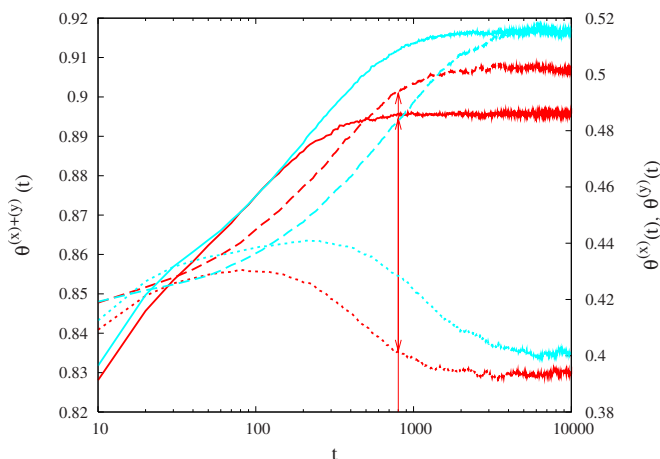


FIG. 2. (Color online) Shown here is the time dependence of the coverage fraction for mixture (C)+(D) (see Table II) and its components for $r^{(C)}=r^{(D)}=1/2$ and for two different values of desorption probability $P_- = 0.002, 0.001$. Black (red) and gray (light blue) lines represent the results obtained for $P_- = 0.002$ and 0.001 , respectively. The solid lines represent the temporal behavior of coverage fraction $\theta^{(C)+(D)}(t)$ (left-hand axis). The dashed and dotted lines are plotted against the right-hand axis and give the coverage fraction versus time t of component shapes (D), $\theta^{(D)}(t)$ (dashed line), and (C), $\theta^{(C)}(t)$ (dotted line). Thin vertical arrow indicates the beginning of the equilibrium plateau in the time evolution of the coverage fraction $\theta^{(C)+(D)}(t)$ for $P_- = 0.002$.

shapes, for $r^{(B)}=r^{(C)}=1/2$ and for two values of $P_- = 0.002, 0.001$. For the shape (B) of higher order of symmetry $n_s^{(B)} = 2$, the coverage $\theta^{(B)}(t)$ is a monotonously increasing function of time and has the same general features as the coverage $\theta^{(B)+(C)}(t)$ for mixture (B)+(C). On the other hand, for the shape (C) of lower order of symmetry $n_s^{(C)} = 1$, the coverage $\theta^{(C)}(t)$ is not monotonic in time. When the coverage $\theta^{(B)+(C)}(t)$ approaches to the coverage fraction that is equal to the jamming limit $\theta_{\text{jam}}^{(B)+(C)} = 0.8526$, the coverage $\theta^{(C)}(t)$ reaches a broad maximum. This is followed by a slow relaxation of $\theta^{(C)}(t)$ to the smaller steady-state value $\theta_{\infty}^{(C)}$. The results show a strong dependence of the maximum of $\theta^{(C)} \times (t)$ on the desorption probability P_- . One clearly observes (i) that a larger value for the maximum of the coverage $\theta^{(C)}(t)$ is reached for the smaller desorption probability P_- and (ii) that the maximum of $\theta^{(C)}(t)$ shifts towards larger times as the desorption probability P_- decreases.

The temporal evolutions of the total coverages $\theta^{(C)+(D)}(t)$ and $\theta^{(B)+(D)}(t)$ for the reversible RSA of mixtures (C)+(D) and (B)+(D) are shown in Figs. 2 and 3, respectively. Also included in Figs. 2 and 3 are the time dependences of the coverages $\theta^{(B)}(t)$, $\theta^{(C)}(t)$, and $\theta^{(D)}(t)$ for each mixture component, i.e., for the shapes (B), (C), and (D). The simulations were carried out with the parameters $r^{(B)}=r^{(C)}=r^{(D)}=1/2$ and $P_- = 0.002, 0.001$. These results confirm that, for sufficiently high coverages, the large times coverage fraction of more symmetric shapes exceeds the coverage fraction of less symmetric ones. The steady-state value of the coverage fraction is always larger for the shapes with the symmetry axis of higher order n_s .

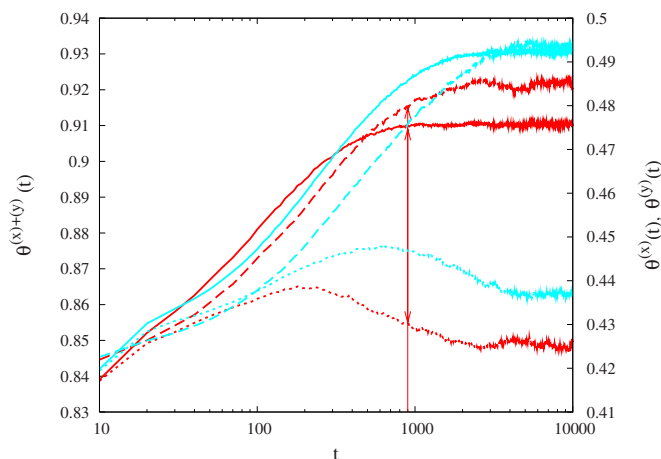


FIG. 3. (Color online) Shown here is the time dependence of the coverage fraction for mixture (B)+(D) (see Table II) and its components for $r^{(B)}=r^{(D)}=1/2$ and for two different values of desorption probability $P_- = 0.002, 0.001$. Black (red) and gray (light blue) lines represent the results obtained for $P_- = 0.002$ and 0.001 , respectively. The solid lines represent the temporal behavior of coverage fraction $\theta^{(B)+(D)}(t)$ (left-hand axis). The dashed and dotted lines are plotted against the right-hand axis and give the coverage fraction versus time t of component shapes (D), $\theta^{(D)}(t)$ (dashed line), and (B), $\theta^{(B)}(t)$ (dotted line). Thin vertical arrow indicates the beginning of the equilibrium plateau in the time evolution of the coverage fraction $\theta^{(B)+(D)}(t)$ for $P_- = 0.002$.

A qualitative interpretation of these results can be attained by exploiting the above-mentioned picture of multiparticle transitions for governing the late-time changes in the coverage fraction $\theta^{(x)+(y)}(t)$. In the following, we assume that the ratio $K = P_+/P_-$ is large enough to ensure that the system of adsorbed particles evolves continuously toward an equilibrium disordered state. In the initial stages of the process, desorption events are negligible compared with adsorption and the process displays an RSA-like behavior. When the value of $\theta_{\text{jam}}^{(x)+(y)}$ is reached, the rare desorption events are generally followed by immediate readsorption. Therefore, the total number of particles is not changed by these *single-particle* events. However, when one badly sited object desorbs and two particles adsorb in the opened good location, then the number of particles is increased by one. Likewise, if two well sited objects desorb and a single object adsorbs in their stead, the number of particles is decreased by one. These *collective* events are responsible for the density growth above $\theta_{\text{jam}}^{(x)+(y)}$ [5,19]. At late enough time, when the coverage fraction is sufficient to make the geometry of the unoccupied sites complex, there is a strong dependence of the adsorption rate on the adsorbed shape [8,12]. At large times, adsorption events take place on isolated islands of connected unoccupied sites. The individual islands have well-defined positions and orientations for adsorption to take place and act as selective targets for specific occupation events. The symmetry properties of the shapes have a significant influence on the filling of small isolated targets on the lattice. Indeed, there is only a restricted number of possible orientations in which an object can reach a previously opened location, provided the location is small enough. For a

shape with a symmetry axis of higher order there is a greater number of possible orientations for deposition into an isolated location at the lattice. Hence, the increase of the order of symmetry of the shape enhances the rate of single particle adsorption. In principle, the adsorption of asymmetric shapes is slower than the adsorption of more regular and symmetric shapes. This is reflected in the gradual decrease of the coverage fraction with time for the shape with the symmetry axis of lower order, as seen in Figs. 1–3.

One striking feature of Figs. 1–3 is the fact that the steady-state value $\theta_{\infty}^{(x)+(y)}$ of the total coverage fraction $\theta^{(x)+(y)}(t)$ was reached before the coverages $\theta^{(x)}(t)$ and $\theta^{(y)}(t)$ achieved their asymptotic values $\theta_{\infty}^{(x)}$ and $\theta_{\infty}^{(y)}$. Each of the thin vertical lines in Figs. 1–3 indicates the beginning of the equilibrium plateau in the time evolution of the coverage fraction $\theta^{(x)+(y)}(t)$. Note that in this regime, the coverage fraction of the mixture fluctuates around its steady-state value $\theta_{\infty}^{(x)+(y)}$, but the coverage fraction of the shape with the symmetry axis of higher order continues to grow at the expense of the coverage of the component with the symmetry axis of lower order, that decreases. Very close to the equilibrium and for large values of $K=P_+/P_-$, the two-particle events contribution to the dynamics decreases dramatically [5]. Then the adsorption and desorption events can be considered as spatially uncorrelated [7], and the system can be represented as a set of independent targets on the lattice in which a particle is adsorbed or not. In this late stage, RSA acts to preferentially adsorb the more symmetric shapes from the reservoir. This is a consequence of the fact that unlike for the less symmetric objects, much more orientations are allowed for regular and symmetric shapes falling in the isolated selective target spaces. For the coverages close to the steady-state value $\theta_{\infty}^{(x)+(y)}$, both rotational symmetry of the shapes and desorption events manage the single-particle readsorptions on the lattice and, eventually, allow replacements of the less symmetric particles by the more symmetric ones. Fine tuning of incoming and outgoing flux of each component is occurred during this final stage. RSA acts to preferentially adsorb the more regular shape from the reservoir, but higher value of its coverage fraction enhances the frequency of desorption events. Moreover, the less symmetric shape adsorbs less efficiently than the symmetric one, but lower value of its coverage fraction decreases the frequency of desorption events. The presence of the above described mechanism, i.e., competing desorption and adsorption of component shapes, implies that each mixture component reaches a steady state in which the adsorption flux is exactly balanced by the desorption flux.

We have also performed a set of numerical simulations using large shapes of length $\ell=6$ that occupy seven lattice sites. Figure 4 shows the time dependence of the coverage fraction for mixtures $(I)+(J)$ and $(J)+(K)$ (see Table II) and its components obtained by the simulations carried out with the parameters $r^{(I)}=r^{(J)}=r^{(K)}=1/2$ and $P_-=0.002$. As it can be seen, a larger steady-state value of the total coverage fraction $\theta_{\infty}^{(x)+(y)}$ is reached by the reversible RSA process involving the rodlike shapes (I) (7-mers) compared with a similar process involving the angled objects (K) . In both mixtures, the coverage fraction of highly symmetric shape (J) exceeds

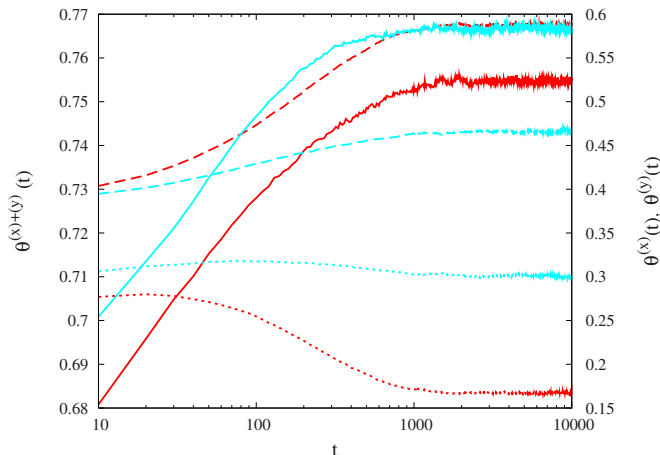


FIG. 4. (Color online) Shown here is the time dependence of the coverage fraction for mixtures $(I)+(J)$ and $(J)+(K)$ (see Table II) and their components for $r^{(I)}=r^{(J)}=r^{(K)}=1/2$ and $P_-=0.002$. Black (red) and gray (light blue) lines represent the results obtained for mixtures $(J)+(K)$ and $(I)+(J)$, respectively. The solid lines represent the temporal behavior of coverage fractions $\theta^{(I)+(J)}(t)$ and $\theta^{(J)+(K)}(t)$ (left-hand axis). The dashed and dotted lines are plotted against the right-hand axis and give the coverage fraction versus time t of component shapes (J) , $\theta^{(J)}(t)$ (dashed line), (I) , $\theta^{(I)}(t)$ (dotted line), and (K) , $\theta^{(K)}(t)$ (dotted line).

the coverage fraction of the other, less symmetric, mixture component, at all times. The noticeable drop in the time evolution of the coverage fraction $\theta^{(K)}(t)$ for the angled object (K) is thus a clear consequence of the enhanced frustration of the spatial adsorption. The pattern formed during the reversible RSA is made up of a large number of domains. In the case of the deposition of 7-mers (I) , any such domain contains a large number of objects all close to each other and parallel. However, the growth of domains is substantially frustrated in the case of the angled objects (K) . This is reflected in the relatively low local packing of adsorbed objects in the vicinity of a given object (J) in the case of the angled objects (K) , as compared to the more symmetric 7-mers (I) , resulting in a smaller value of the coverage fraction in the former case.

The simulations described above were augmented by additional simulations that were carried out to explore the dependence of the reversible RSA kinetics of the mixtures on the number of segments of the shapes. Results for mixtures $(A)+(B)$ and $(A)+(E)$ (see Table II) composed of the linear segments (k -mers) of various lengths are shown in Figs. 5 and 6. In Fig. 5 we compare the temporal evolution of the total coverage fraction $\theta^{(A)+(B)}(t)$ for the two values of desorption probability $P_-=0.002, 0.001$. As expected, the asymptotic coverage $\theta_{\infty}^{(A)+(B)}$ is higher for the lower desorption probability $P_-=0.001$. On the other hand, the coverage fraction $\theta^{(A)}(t)$ of dimers (A) exceeds the coverage fraction $\theta^{(B)}(t)$ of the larger shapes (B) at all times. The reasons for these results are intuitively clear. Due to the fact that the densification kinetics is dictated by geometric exclusion effects, in the competition for adsorption between the two species of different number of segments the smaller shapes win.

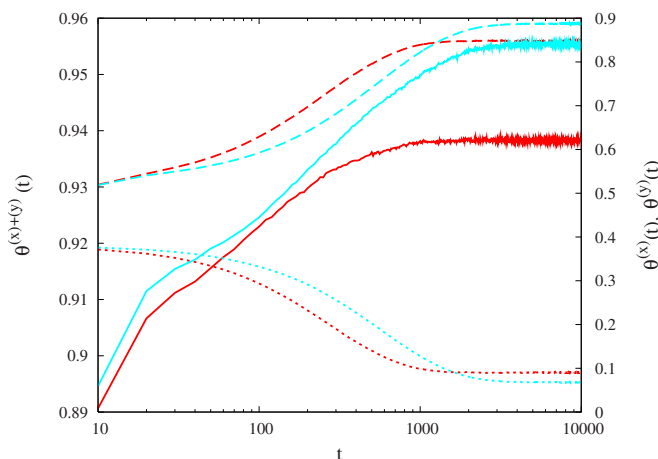


FIG. 5. (Color online) Shown here is the time dependence of the coverage fraction for mixture (A)+(B) (see Table II) and its components for $r^{(A)}=r^{(B)}=1/2$ and for two different values of desorption probability $P_- = 0.002, 0.001$. Black (red) and gray (light blue) lines represent the results obtained for $P_- = 0.002$ and 0.001 , respectively. The solid lines represent the temporal behavior of coverage fraction $\theta^{(A)+(B)}(t)$ (left-hand axis). The dashed and dotted lines are plotted against the right-hand axis and give the coverage fraction versus time t of component shapes (A), $\theta^{(A)}(t)$ (dashed line), and (B), $\theta^{(B)}(t)$ (dotted line).

Moreover, the larger shapes desorb much more efficiently than the smaller ones, that leads to the higher coverage fraction of the smaller species. From Fig. 6 it is evident that for small values of desorption probability P_- , the dynamics of mixture (A)+(E) close to the steady-state limit $\theta_{\infty}^{(A)+(E)}$ is entirely governed by the dynamics of the smaller species (A).

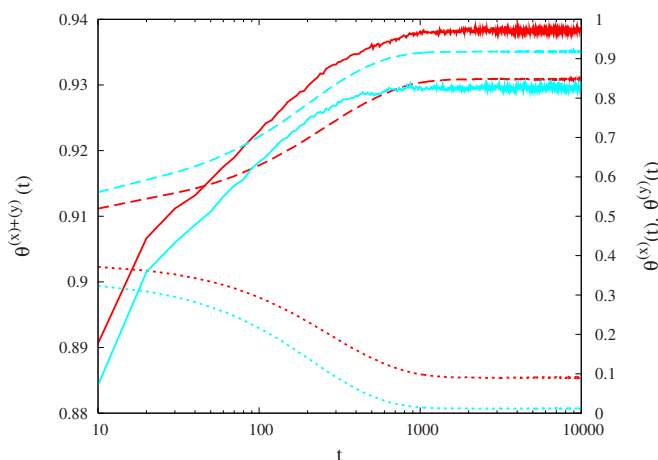


FIG. 6. (Color online) Shown here is the time dependence of the coverage fraction for mixtures (A)+(B) and (A)+(E) (see Table II) and their components for $r^{(A)}=r^{(B)}=r^{(E)}=1/2$ and $P_- = 0.002$. Black (red) and gray (light blue) lines represent the results obtained for mixtures (A)+(B) and (A)+(E), respectively. The solid lines represent the temporal behavior of coverage fractions $\theta^{(A)+(B)}(t)$ and $\theta^{(A)+(E)}(t)$ (left-hand axis). The dashed and dotted lines are plotted against the right-hand axis and give the coverage fraction versus time t of component shapes (A), $\theta^{(A)}(t)$ (dashed line), (B), $\theta^{(B)}(t)$ (dotted line), and (E), $\theta^{(E)}(t)$ (dotted line).

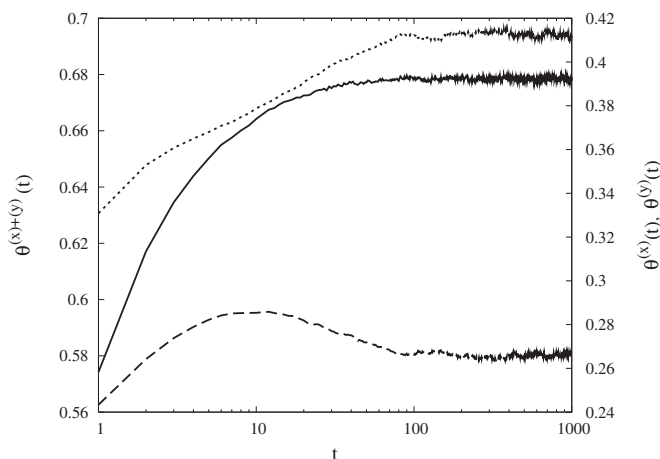


FIG. 7. Shown here is the time dependence of the coverage fraction for mixture (J)+(H) (see Table II) and its components for $r^{(J)}=r^{(H)}=1/2$ and $P_- = 0.01$. The solid lines represent the temporal behavior of coverage fraction $\theta^{(J)+(H)}(t)$ (left-hand axis). The dashed and dotted lines are plotted against the right-hand axis and give the coverage fraction versus time t of component shapes (J), $\theta^{(J)}(t)$ (dotted line), and (H), $\theta^{(H)}(t)$ (dashed line).

The contribution of the larger shape (E) to the total coverage fraction $\theta^{(A)+(E)}(t)$ does not vanish for large times, but it becomes negligible.

Figure 7 puts into evidence a somewhat counterintuitive feature for the case of reversible deposition of polydisperse mixtures. At high coverages the contribution of the mixture components to the total coverage fraction is found to be larger for the larger shapes than for the smaller ones. In Fig. 7 we present the reversible RSA kinetics of mixture (J)+(H) (see Table II) for the desorption probability $P_- = 0.01$ and for $r^{(J)}=r^{(H)}=1/2$. The shapes (J) and (H) occupy seven and six lattice sites, respectively, and therefore introduce a size bidispersity into the deposition phenomena. Moreover, the results shown in Figs. 1–4 suggest that the rotational symmetries associated with specific shapes have a substantial influence on the adsorption rate of the mixture components. Shapes (J) and (H) have the order of symmetry axis equal to $n_s = 6$ and $n_s = 1$, respectively. The great symmetry order difference between the larger and the smaller particles in the bidisperse mixtures provides the predominance of the larger shapes in the total coverage at all times.

IV. COMPOSITION DEPENDENCE OF THE STEADY-STATE COVERAGE FRACTION

The purpose of this section is to find an expression for the steady-state coverage fraction of mixture in terms of the steady-state coverage fractions of pure lattice shapes. To our knowledge, there are very few works concerning this topic. Theoretical effort was restricted only to a binary mixture of particles with very large size differences [14,20,21]. Talbot and Schaaf [20] analyzed the irreversible adsorption of mixtures of hard disks of greatly differing diameters. They found that the jamming limit $\theta_{\text{jam}}^{(S)+(L)}$ of the mixture of small (S) and large (L) disks is accurately given by

$$\theta_{\text{jam}}^{(S)+(L)} = \theta_{\text{jam}}^{(L)} + 0.547[1 - (1 + \lambda)^2 \theta_{\text{jam}}^{(L)}], \quad (4.1)$$

where $\theta_{\text{jam}}^{(L)}$ is the jamming limit of large disk (L) when deposited from the mixture, $\lambda = \sigma_S / \sigma_L$ is the diameter ratio, and 0.547 is the jamming coverage corresponding to the irreversible RSA of equal sized disks on a continuous surface.

Like many other statistical-mechanical problems, exact solutions for the steady-state coverage and for the kinetics of the reversible RSA process in one-component systems exist only in one dimension [4,22,23]. Furthermore, to date there is no exact analytical solution for the reversible RSA process in mixtures of a finite number of species. Therefore, much of the information about the reversible RSA kinetics of mixtures in higher dimensions is provided by numerical simulations or by experiment. We have analyzed the simulation data in order to find a dependence of the steady-state coverage fraction of a mixture on the steady-state coverage fractions of pure lattice shapes. We propose the following simple formula for calculating the steady-state coverage fraction $\theta_{\infty}^{(x)+(y)}$ in the mixture $(x)+(y)$ of equal sized shapes (x) and (y) with fractional concentrations $r^{(x)}$ and $r^{(y)} = 1 - r^{(x)}$ in the infinite reservoir:

$$\frac{1}{\theta_{\infty}^{(x)+(y)}} = r^{(x)} \frac{1}{\theta_{\infty}^{(x)}} + r^{(y)} \frac{1}{\theta_{\infty}^{(y)}}, \quad (4.2)$$

where $\theta_{\infty}^{(x)}$ and $\theta_{\infty}^{(y)}$ are the steady-state coverage fractions of pure lattice shapes. Equation (4.2) shows that the reciprocal of the steady-state coverage fraction of a mixture changes linearly with the concentration of a component shape in the reservoir.

Formula (4.2) is supported by a good agreement with the numerical simulations. We have numerically tested whether this formula can be used to predict the value of a steady-state coverage fraction of a mixture from the values of the steady-state coverage fractions of pure component shapes. Figure 8 compares the steady-state coverage fraction $\theta_{\infty}^{(x)+(y)}$ of mixtures $(x)+(y)=(B)+(D)$, $(C)+(D)$, and $(F)+(G)$ (see Table II) as a function of the desorption probability P_- with the values obtained using Eq. (4.2). Objects are deposited from the reservoir which contains the shapes (x) and (y) with fractional concentrations $r^{(x)}=0.8$ and $r^{(y)}=0.2$, respectively. Closed symbols refer to the data obtained from the numerical simulations, and the results obtained from Eq. (4.2) are shown for comparison as opened symbols. One clearly observes that Eq. (4.2) excellently well predicts the values of $\theta_{\infty}^{(x)+(y)}$ from the values of the steady-state coverage fraction of pure component shapes $\theta_{\infty}^{(x)}$ and $\theta_{\infty}^{(y)}$, in the whole range of desorption probability P_- considered.

In Figs. 9–11 we show the results obtained for various compositions of mixtures $(x)+(y)=(B)+(D)$, $(C)+(D)$, and $(F)+(G)$ (see Table II). For each value of $r^{(x)}/r^{(y)}=0.6/0.4$, $0.5/0.5$, and $0.4/0.6$, simulations were carried out for various values of the parameter P_- . Once again we observe that the values of the steady-state coverage fraction of a mixture calculated using Eq. (4.2) agree very well with the simulation results. The deviation is up to 0.1% for mixtures $(B)+(D)$ and $(C)+(D)$ and up to 2% for mixture $(F)+(G)$. Namely, the data shown in Figs. 9–11 for mixture $(F)+(G)$

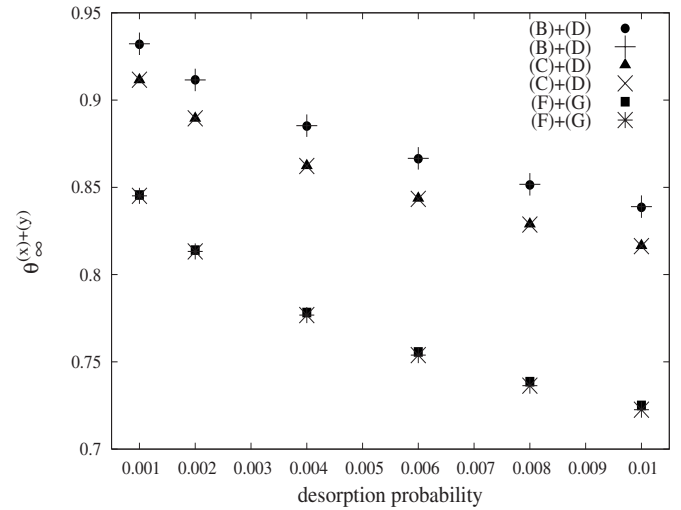


FIG. 8. Plot of the steady-state coverage fraction $\theta_{\infty}^{(x)+(y)}$ against desorption probability P_- for mixtures $(x)+(y)=(B)+(D)$, $(C)+(D)$, and $(F)+(G)$ (see Table II). Fractional concentrations of the shapes (x) and (y) in the reservoir are $r^{(x)}=0.80$ and $r^{(y)}=0.20$. Closed symbols refer to the data obtained from the numerical simulations. Open symbols are the steady-state coverages $\theta_{\infty}^{(x)+(y)}$ calculated from Eq. (4.2).

indicate that the values of $\theta_{\infty}^{(F)+(G)}$ calculated using Eq. (4.2) deviate slightly from our simulation results, especially at low values of desorption probability P_- . A possible reason for this difference could lie in the inaccuracy of the numerically determined steady-state values of the coverage fraction $\theta_{\infty}^{(G)}$ for large and highly symmetric object (G) at low values of desorption probability P_- . Recently we have shown [8] that the time coverage behavior is severely slowed down with the

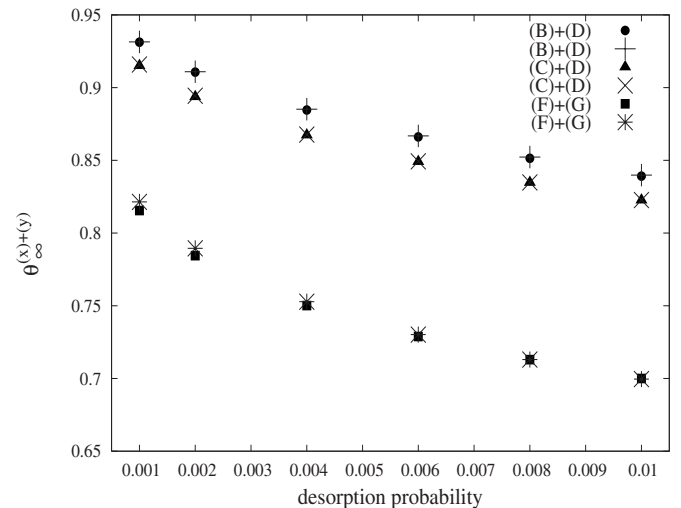


FIG. 9. Plot of the steady-state coverage fraction $\theta_{\infty}^{(x)+(y)}$ against desorption probability P_- for mixtures $(x)+(y)=(B)+(D)$, $(C)+(D)$, and $(F)+(G)$ (see Table II). Fractional concentrations of the shapes (x) and (y) in the reservoir are $r^{(x)}=0.60$ and $r^{(y)}=0.40$. Closed symbols refer to the data obtained from the numerical simulations. Open symbols are the steady-state coverages $\theta_{\infty}^{(x)+(y)}$ calculated from Eq. (4.2).

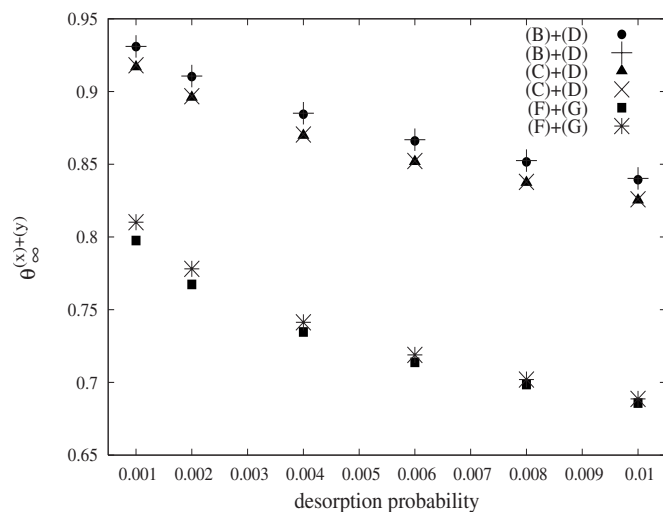


FIG. 10. Plot of the steady-state coverage fraction $\theta_{\infty}^{(x)+(y)}$ against desorption probability P_- for mixtures $(x)+(y)=(B)+(D)$, $(C)+(D)$, and $(F)+(G)$ (see Table II). Fractional concentrations of the shapes (x) and (y) in the reservoir are $r^{(x)}=0.50$ and $r^{(y)}=0.50$. Closed symbols refer to the data obtained from the numerical simulations. Open symbols are the steady-state coverages $\theta_{\infty}^{(x)+(y)}$ calculated from Eq. (4.2).

increase of the order of rotational symmetry of the shape. Hence, the time required to achieve the steady state increases with the symmetry order. Likewise, the dynamics of reversible RSA gets drastically slower when the desorption probability decreases. Unfortunately, we do not have a sufficient computing power to precisely determine the steady-state values of coverage fraction $\theta_{\infty}^{(G)}$ for the shape G . Nevertheless, the agreement between the calculated values for θ_{∞} for the mixtures and the results obtained by numerical simulations is very good.

V. CONCLUDING REMARKS

We have performed extensive numerical simulations of the reversible RSA using binary mixtures composed of the shapes of different number of segments and rotational symmetries on a triangular lattice. The shapes are made by self-avoiding lattice steps. A systematic approach is made by examining a wide variety of object shapes and their mixtures.

The simulations have shown that the coverage kinetics of a mixture strongly depends on the symmetry properties of the component shapes. It has been shown that, for sufficiently large times, the coverage fraction of more symmetric shapes exceeds the coverage fraction of less symmetric ones. We have also highlighted the significance of collective events for governing the time coverage behavior of compo-

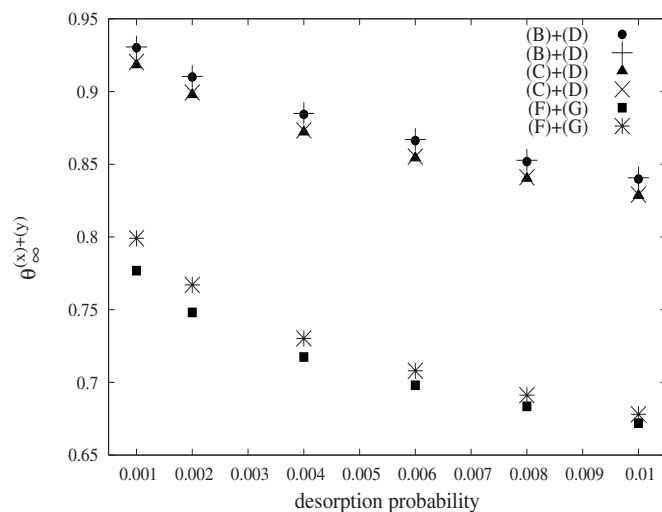


FIG. 11. Plot of the steady-state coverage fraction $\theta_{\infty}^{(x)+(y)}$ against desorption probability P_- for mixtures $(x)+(y)=(B)+(D)$, $(C)+(D)$, and $(F)+(G)$ (see Table II). Fractional concentrations of the shapes (x) and (y) in the reservoir are $r^{(x)}=0.40$ and $r^{(y)}=0.60$. Closed symbols refer to the data obtained from the numerical simulations. Open symbols are the steady-state coverages $\theta_{\infty}^{(x)+(y)}$ calculated from Eq. (4.2).

nent shapes with different rotational symmetries.

Furthermore, the coverage kinetics of a mixture has a rich behavior in comparison to that of a reversible deposition of pure lattice shapes. From our results we can identify a new regime for the reversible RSA in the mixtures of objects of different symmetries that has no counterpart in single component systems. In this regime, the coverage fraction of a mixture fluctuates around its steady-state value, but the coverage fraction of the shape with the symmetry axis of higher order continues to grow at the expense of the coverage of the component with the symmetry axis of lower order.

We have proposed a simple formula (4.2) that can be used to predict the value of a steady-state coverage fraction of a mixture from the values of the steady-state coverage fractions of pure component shapes. This is important because the numerical simulations of the reversible RSA of mixtures are very time consuming. It is clear that analytic work is needed to fully explore the range of validity and conditions under which Eq. (4.2) can be established. However, any theoretical treatment of this problem is necessarily very complex and it is beyond the scope of this paper.

ACKNOWLEDGMENT

This research was supported by the Ministry of Science of the Republic of Serbia, under Grant No. 141035.

- [1] J. W. Evans, *Rev. Mod. Phys.* **65**, 1281 (1993).
- [2] V. Privman, *Colloids Surf., A* **165**, 231 (2000).
- [3] B. Senger, J. C. Voegel, and P. Schaaf, *Colloids Surf., A* **165**, 255 (2000).
- [4] J. Talbot, G. Tarjus, P. R. Van Tassel, and P. Viot, *Colloids Surf., A* **165**, 287 (2000).
- [5] R. S. Ghaskadvi and M. Dennin, *Phys. Rev. E* **61**, 1232 (2000).
- [6] E. Frey and A. Vilfan, *Chem. Phys.* **284**, 287 (2002).
- [7] J. Talbot, G. Tarjus, and P. Viot, *Phys. Rev. E* **61**, 5429 (2000).
- [8] Lj. Budinski-Petković, M. Petković, Z. M. Jakšić, and S. B. Vrhovac, *Phys. Rev. E* **72**, 046118 (2005).
- [9] D. Arsenović, S. B. Vrhovac, Z. M. Jakšić, Lj. Budinski-Petković, and A. Belić, *Phys. Rev. E* **74**, 061302 (2006).
- [10] G. Tarjus and P. Viot, *Phys. Rev. E* **69**, 011307 (2004).
- [11] Lj. Budinski-Petković and S. B. Vrhovac, *Eur. Phys. J. E* **16**, 89 (2005).
- [12] Lj. Budinski-Petković and U. Kozmidis-Luburić, *Phys. Rev. E* **56**, 6904 (1997).
- [13] M. N. Berberan-Santos, *J. Mater. Chem.* **38**, 629 (2005).
- [14] M. C. Bartelt and V. Privman, *Phys. Rev. A* **44**, R2227 (1991).
- [15] S. S. Manna and N. M. Švrakić, *J. Phys. A* **24**, L571 (1991).
- [16] Lj. Budinski-Petković and U. Kozmidis-Luburić, *Physica A* **236**, 211 (1997).
- [17] J. W. Lee, *Physica A* **331**, 531 (2004).
- [18] Lj. Budinski-Petković and T. Tošić, *Physica A* **329**, 350 (2003).
- [19] A. J. Kolan, E. R. Nowak, and A. V. Tkachenko, *Phys. Rev. E* **59**, 3094 (1999).
- [20] J. Talbot and P. Schaaf, *Phys. Rev. A* **40**, 422 (1989).
- [21] G. Tarjus and J. Talbot, *Phys. Rev. A* **45**, 4162 (1992).
- [22] P. L. Krapivsky and E. Ben-Naim, *J. Chem. Phys.* **100**, 6778 (1994).
- [23] G. Tarjus, P. Schaaf, and J. Talbot, *J. Chem. Phys.* **93**, 8352 (1990).